Acoustic phonons and a central mode in the protonic conductor $K_3H(SeO_4)_2$

Fumihito Shikanai,* Shinya Tsukada, Jun Kano, and Seiji Kojima†
Graduate School of Pure and Applied Sciences, University of Tsukuba, Tsukuba, Ibaraki 305-8573, Japan
(Received 1 September 2009; revised manuscript received 8 October 2009; published 12 January 2010)

The dynamical properties of protonic conductor $K_3H(SeO_4)_2$ were examined by Brillouin scattering. Both longitudinal-acoustic modes (c_{33} and c_{11}) and a transversal mode (c_{44}) monotonously depend on temperature, and no soft mode was observed. A central mode with a width about 6 GHz was observed above phase-transition temperature, T_C. The central mode has a symmetry E_g corresponding to the rotational mode of SeO_4 tetrahedra. The E_g mode is compatible with a zone-boundary soft mode, L_3, which accounts for the symmetrical change from $R\bar{3}m$ to $C2/c$. The intensity of the central mode declines in the vicinity of T_C. This shows that chaotic rotational motion changes into a zone-boundary soft mode with decreasing temperature.

DOI: 10.1103/PhysRevB.81.012301 PACS number(s): 66.30.H−, 77.84.Fa, 78.35.+c

Development of solid electrolytes for fuel cells that work at a medium temperature range is desired. Oxide ceramics used in a solid oxide fuel cells (SOFCs) show self-catalysis at operating temperatures greater than 600 °C. Because the electrical energy is transformed from the chemical reaction energy of oxygen and hydrogen, high-temperature operation is preferable. However, at high temperatures, problems such as the deterioration of electrodes occur. On the other hand, a polymer electrolyte membrane (PEM) shows marked high electrical conductivity of more than 10^{-2} S/cm. However, PEMs must be operated below 100 °C because the protons are transferred by water. Some hydrogen-bonded anhydrous materials represented as $MHXO_4$ and $M_3H(XO_4)_2$ (M=K,Rb,Cs, NH_4 and X=S,Se) may attempt to solve this problem. Most of them undergo phase transitions above 150 °C and show high electrical conductivity of about 10^{-3} to 10^{-2} S/cm without decomposition even in humid atmosphere despite their water solubility.[1] Application of their proton conduction mechanism to a new solid electrolyte is expected to facilitate development of a next-generation fuel cell; therefore, the clarification of the mechanism is required urgently.

$K_3H(SeO_4)_2$ (TKHSe) is one of the $M_3H(XO_4)_2$-type compounds that has been investigated in terms of the phase-transition mechanism for years.[2–7] The material undergoes a first-order phase transition at 390 K (T_C); it shows a remarkably high electrical conductivity of about 10^{-3} S/cm, above T_C (phase I) and is ferroelastic below T_C (phase II).[8] The crystal belongs to the trigonal system with the space group $R\bar{3}m$ in phase I and to monoclinic $C2/c$ in phase II. An isolated SeO_4-H-SeO_4 dimer characterizes the crystal structure in phase II,[9,10] and no interdimer hydrogen bond exists. The dimers construct a layered structure parallel to the monoclinic b_mc_m-plane [see Figs. 3(d) and 3(e)] and form a deformed hexagon by the pseudo $\bar{3}$ axis, which is perpendicular to the plane. The hydrogen bonds form a herringbone pattern in the layer in the direction c_m+b_m or c_m-b_m; no pattern exists in the direction $-c_m$. In phase I, the distances from a SeO_4 tetrahedron to the nearest three tetrahedra are equivalent; and a tetrahedron is linked to one of them with a probability 1/3.[11,12] Many proton transfer models that show disconnection and reconstruction of hydrogen bond accompanied by the deformation[13–16] or rotation[17] of tetrahedra have been proposed. However, the evidence for the dynamical properties of tetrahedra have not been reported in detail.

In addition, the crystal structure in phase II is the superlattice structure of that in phase I. The lattice interval in the direction of trigonal b_t in phase II modulates to twice that in phase I. This shows that the ferroelastic phase transition is an improper type occurring at the zone-boundary L-point 0 k/2 0.[18] Recently, we performed inelastic neutron-scattering (INS) (Ref. 11) and quasielastic neutron-scattering (QENS) (Ref. 19) experiments on TKHSe. From INS, a broad spectrum was observed around 0 meV at L point 0.5 2 0 in phase I. The spectrum increases and narrows with decreasing temperature and accounts for the soft mode by an overdamped rotational tetrahedra mode. The full width at half maximum (FWHM) is 70(6) μeV at 435 K. On the other hand, from QENS, a spectrum due to the large incoherent-scattering length of proton was observed. The FWHM of the spectrum depends on both temperature and scattering vector, Q; the maximum value estimated from deconvolution of instrumental function is 20(12) μeV at 413 K and 1.65 Å^{-1}. What needs to be emphasized is that both spectra have been observed at extremely low energy, within 100 μeV (24.2 GHz). This indicates that similar excitation in the low-energy region by protons or tetrahedra also exist at the Γ point. Furthermore, the temperature dependence of the acoustic mode in the vicinity of the Γ point is important for characterizing the ferroelastic phase transition. Therefore, we performed Brillouin scattering experiment on TKHSe, which has high resolution and signal-to-noise ratio.

The present Brief Report reports the acoustic and central mode (CM) of TKHSe in the low-energy region. We show the temperature dependence of the acoustic mode, which is closely related to the ferroelastic phase transition. In addition, we show details of the CM found above T_C and discuss its origin based on its symmetry and temperature dependence.

Single crystals of TKHSe were grown at 313 K from an aqueous solution by slow evaporation method. A transparent singlecrystal $1.3\times1.0\times0.9$ mm^3 in size was used as a specimen. The light source was a diode-pumped solid-state laser with a single frequency, λ=532 nm. Light-scattering measurements were performed using a high-contrast 3+3-pass tandem Fabry-Pérot interferometer (JRS Science

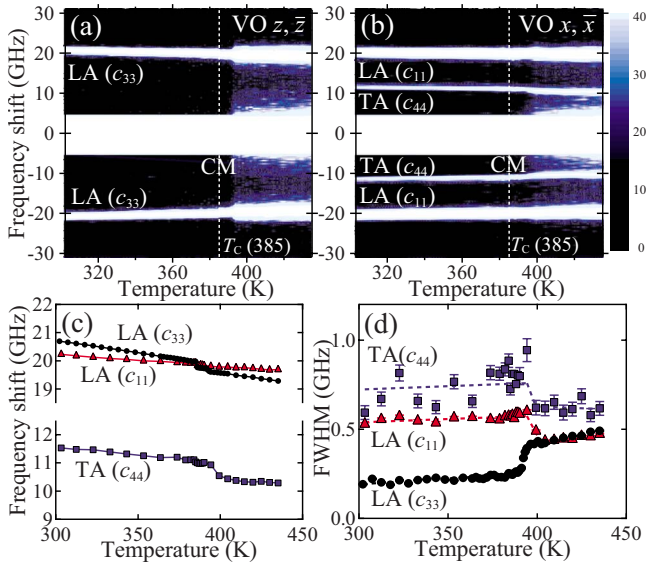

FIG. 1. (Color online) Temperature dependence of inelastic light scattering of $K_3H(SeO_4)_2$. (a) VO $z, \bar{z}$. (b) VO $x, \bar{x}$. (c) Frequency shift of acoustic mode. (d) FWHM of acoustic mode.

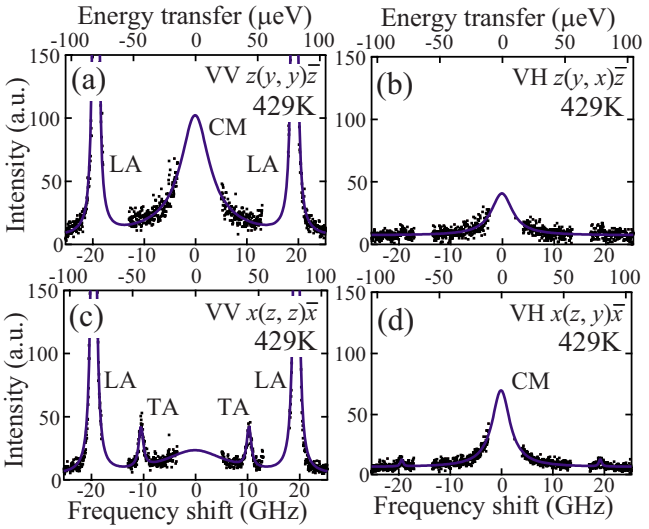

FIG. 2. (Color online) The polarization character of CM at 429 K. (a) VV $z(y,y)\bar{z}$. (b) VH $z(y,x)\bar{z}$. (c) VV $x(z,z)\bar{x}$. (d) VH $x(z,y)\bar{x}$.

Instruments)[20] and found a 180° scattering geometry, under polarization conditions without a polarizer [vertical to open (VO)], for the acoustic mode. The data were recorded during cooling at various temperatures from 435 to 300 K. An additional experiment has been performed to measure the CM above T_C. Two other polarization conditions, parallel polarizer [vertical to vertical (VV)] and cross polarizer [vertical to horizontal (VH)], were used to examine the symmetry of the CM spectrum at 429 K. The phase-transition temperature T_C was 385 K due to thermal hysteresis during cooling measurement. The lattice axes with no subscript described in the text are those of a trigonal cell (hexagonal setting) in phase I, and x, y, and z were defined as $x=a+b=b_m$, $y=b-a=c_m$, and $z=c=a_m^*$, respectively. The relationship between the hexagonal and trigonal settings are $a=a_t-b_t$, $b=b_t-c_t$, and $c=a_t+b_t+c_t$.

Figure 1(a) and 1(b) shows the contour maps of light-scattering intensity versus frequency shift and temperature. A longitudinal-acoustic (LA) mode is observed at the frequency shift $\pm 20.691(1)$ GHz at 303 K [Fig. 1(a)]. From Christoffel's equation, $\rho v^2 \pi_i = c_{ijkl} a_j \pi_k a_l$ $(i,j,k,l=1,2,3)$, the LA mode is assigned as a pure longitudinal wave relating to the stiffness c_{33}, where π_i and a_i are the polarizing vector and unit scattering vector, respectively. Similarly, a LA and a transversal acoustic (TA) mode were observed at the frequency shift $\pm 20.234(4)$ and $\pm 11.53(2)$ GHz, respectively, at 303 K [Fig. 1(b)]. Similar calculation shows that the LA mode is the pure longitudinal wave related to c_{11} and the TA mode is a quasitransversal wave $c_{44}+\Delta \simeq c_{44}$, where $\Delta = c_{14}^2\{4(c_{44}-c_{66})\}^{-1}$ under the conditions $c_{14} \ll c_{44}-c_{66}$ and $c_{66}=(c_{11}-c_{12})/2$. Hence, the main diagonal components of the stiffness for $R\bar{3}m$ (c_{11}, c_{33}, and c_{44}) were measured under these scattering geometries.

A Voigt function was used to analyze these spectrum. The FWHM of the Gaussian component was fixed as the instrumental function 0.4698(2) GHz. The temperature dependence of the frequency shift of each acoustic mode is shown in Fig. 1(c). The frequency shift, ν_B, of c_{33} monotonously increases with decreasing temperature and breaks at T_C with a frequency shift of about 0.2 GHz. The other acoustic modes, c_{11} and c_{44} show a similar tendency; however, the steps are at a slightly higher temperature, about 400 K. The velocities of LA and TA at 415 K, obtained using the equation $v=\lambda \nu_B (2n)^{-1}$, are 3449.3(2) and 3504.3(4) m/s for c_{11} and c_{33}, respectively, and 1832(2) m/s for c_{44}. Here, the refractivity as that of a typical hydrogen-bonded material, $n=1.5$, was assumed. These values agree with those obtained from dispersion curve by INS,[11] 3130(132) and 1930(15) m/s for LA and TA, respectively. The stiffness at 415 K obtained by substituting these velocities for $c_{ij}=\rho v^2$ is $c_{11}=3.361(3)\times 10^{10}$, $c_{33}=3.748(9)\times 10^{10}$, and $c_{44}=1.024(3)\times 10^{10}$ Pa, where $\rho=3.052$ g/cm.

Figure 1(d) shows the temperature dependence of the FWHM of the acoustic modes. The FWHM of c_{33} decreases with decreasing temperature and is narrow (0.17 GHz) at T_C. Assuming that the reactivity scarcely depends on temperature, the damping constant of c_{33} at 435 K is 2.76(5) times that at 303 K. The dependence of c_{11} contrasts with that of c_{33}. It agrees with that of c_{33} above T_C but broadens below T_C. The dependence on c_{44} shows a similar tendency. This broadening of c_{11} and c_{44} is considered to indicate split of the signal due to the domain shift during cooling measurement. The hexagonal a in phase I becomes a nonequivalent axis, c_m+b_m, c_m-b_m, or $-c_m$ in phase II, while the hexagonal c, common to both domains, appears as monoclinic a_m^* in phase II. A warming measurement using a single-domain crystal is needed, although a small contribution will be expected for the phase transition. As mentioned above, the acoustic modes depend monotonously on temperature and no soft mode was observed, although the material shows ferroelasticity in phase II.

In addition to these acoustic modes, as shown in both Figs. 1(a) and 1(b), a spectrum of the CM appears within ± 10 GHz above T_C. Figure 2 shows the polarization character of the CM at 429 K. The intensity of the CM is modu-

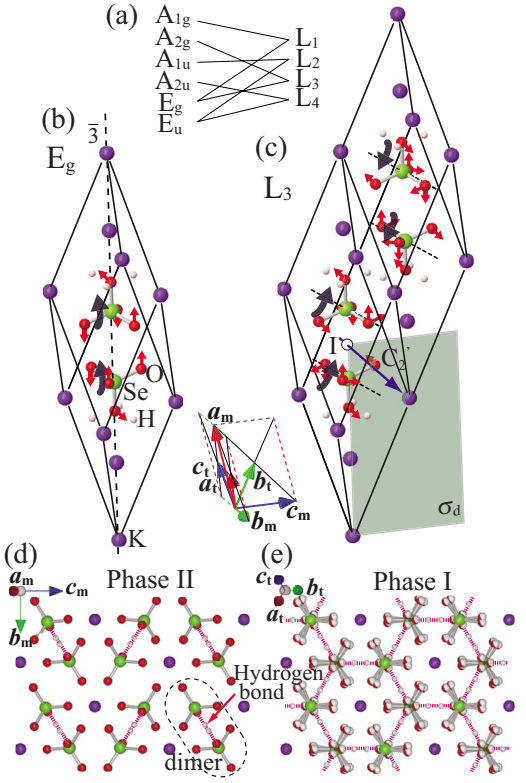

FIG. 3. (Color online) (a) Compatibility conditions between the Γ- and L-point of $R\bar{3}m$. (b), (c) Atomic displacement patterns of E_g and L_3 modes. (d), (e) Hydrogen bond arrangements in the layer in phase II and I, respectively. The structures are illustrated using the atomic positions in Ref. 11

lated under each polarization condition, indicating that the CM is symmetric. The CM spectrum is clearly observed under the polarization conditions in Figs 2(a) and 2(d). In Fig. 2(b), the spectrum significantly decreases, although a small component of CM is remains, which disappears in Fig. 2(c). There exist two types of Raman-active modes for $R\bar{3}m$ (A_{1g} and degenerating E_g). The Raman tensors are given as follows:

$$A_{1g} = \begin{pmatrix} a & 0 & 0 \\ 0 & a & 0 \\ 0 & 0 & b \end{pmatrix}, \quad E_{g1} = \begin{pmatrix} c & 0 & 0 \\ 0 & -c & d \\ 0 & d & 0 \end{pmatrix},$$

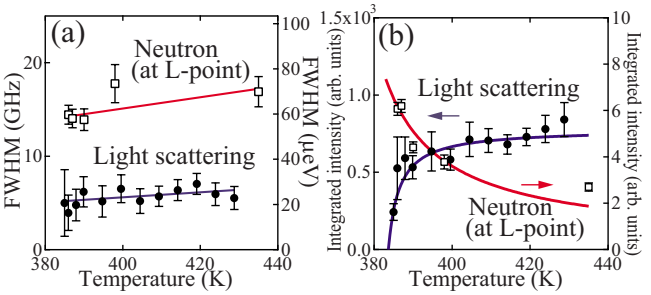

FIG. 4. (Color online) Temperature dependence of CM. (a) FWHM. (b) Integrated intensity. Data denoted by □s are those at the L point obtained by INS (Ref. 11).

$$E_{g2} = \begin{pmatrix} 0 & -c & -d \\ -c & 0 & 0 \\ -d & 0 & 0 \end{pmatrix}. \quad (1)$$

The quadratic form of the incident and scattering polarizing vectors and matrix of E_{g1} gives $-c$, 0, 0, and d for the polarization conditions described in Figs. 2(a)–2(d) (a, 0, b, and 0 for A_{1g} and 0, $-c$, 0, and 0 for E_{g2}). Therefore, the symmetry of the CM is E_{g1}, and the small spectrum in Fig. 2(b) originates from the degenerating mode E_{g2}.

The atomic displacement pattern of E_g mode was obtained by a projection operator at the Γ-point of $R\bar{3}m$, for arbitrary atomic displacements. The result is shown by red arrows in Fig. 3(b). The main symmetry elements of $R\bar{3}m$ are illustrated in Figs. 3(b) and 3(c). The E_g mode is the degenerate rotational mode [Fig. 3(b)]. Two SeO_4 tetrahedra in a unit cell rotate in the same phase, shown as black arrows, and incline in the direction of each hydrogen bond in phase II [see Fig. 3(d)]. On the other hand, from our latest INS experiment, a spectrum having a Lorentz functional shape has been observed around 0 meV at the zone-boundary L point and assigned to the L_3 mode. The definition of L_n is listed in the character table (Table I). Freezing of the L_3 mode accounts for the symmetrical change from $R\bar{3}m$ to maximal subgroup $C2/c$. As illustrated in Fig. 3(c), the L_3 mode also corresponds to the rotational mode of tetrahedra with wavelength $2b_t$. The rotational axes are bisectors of the O-Se-O angles. Figure 3(a) shows the compatibility conditions between the Γ and L points. As described in Fig. 3(a), the E_g representation is compatible with the L_3 representation. Therefore, both the E_g and the L_3 originate from the same family of modes except for those of wavelength. Further-

TABLE I. Character table at L point of $R\bar{3}m$ with maximal sub groups of each irreducible representation.

	E	C_2'	I	σ_d	$\{E\|b_t\}$	$\{C_2'\|b_t\}$	$\{I\|b_t\}$	$\{\sigma_d\|b_t\}$	
L_1	1	1	1	1	−1	−1	−1	−1	$C2/m$
L_2	1	1	−1	−1	−1	−1	1	1	$C2/c$
L_3	1	−1	1	−1	−1	1	−1	1	$C2/c$
L_4	1	−1	−1	1	−1	1	1	−1	$C2/m$

more, the peak shapes and their position, 0 GHz, show that both modes are overdamped.

Figure 4(a) shows the temperature dependence of the FWHM of the CM. The FWHM decreases slightly with temperature from 6.4(1.2) GHz at 429 K to 5.2(1.9) GHz at 386 K. These values correspond to the lifetime of the CM, $1.5(3)\times10^{-10}$ and $1.9(7)\times10^{-10}$ s at 429 and 386 K, respectively. The data denoted by open squares in Fig. 4(a) show the FWHM of spectra at the L-point obtained by INS.[11] The FWHM is 60(4) and 70(6) μeV at 386 and 435 K, respectively, and its lifetimes are $7.1(4)\times10^{-11}$ s to $5.9(4)\times10^{-11}$ s. Although the FWHM values are about 2.5 times larger than that obtained by light scattering because of the resolution of INS, these lifetimes of about 10^{-10} s are consistent with each other. They are also consistent with the relaxation time of transfer protons obtained by other experiments such as NMR in $Rb_3H(SO_4)_2$,[21] 9.54×10^{-10} s at 435 K (the value was calculated from the activation energy, $E_a=25$ KJ^{-1} mol^{-1}, and the inverse of a frequency factor, $\tau_0=9.5\times10^{-13}$ s), and QENS,[19] $4.9(3)\times10^{-11}$ s at 433 K. This shows that proton conduction is simultaneous with the motion of the rotational mode.

Figure 4(b) shows the temperature dependence of the integrated intensity of CM above T_C. The intensity of CM gradually decreases with decreasing temperature and fades out below 400 K. This temperature dependence differs from that of the relaxation mode observed in the representative hydrogen-bonded material KH_2PO_4. The fitting curve used in Fig. 4(b) is $A\{1-BT/(T-T_0)\}$ with three parameters, A, B, and T_0. An extrapolated Curie temperature T_0 of 381(3) K was obtained. The data denoted by open squares in Fig. 4(b) are those at the L point.[11] In contrast to the CM, the data increase with decreasing temperature as $CT/(T-T_0)$, that is, both intensities show complementary temperature dependence. This shows that the overdamped rotational mode is chaotic at sufficiently high temperature, and changes into a zone-boundary phonon mode with decreasing temperature.

In this Brief Report, we showed acoustic and optical excitations of a protonic conductor, TKHSe, in a low-energy region thorough light scattering. Although the material shows ferroelasticity in phase II, both the TA and LA modes show no significant anomaly in a wide temperature region including the vicinity of T_C. On the other hand, a Lorentzian-shaped spectrum with a FWHM of 6 GHz appears around 0 GHz as the CM above T_C. The CM was assigned as an overdamped rotational mode of SeO_4 tetrahedra which has the symmetry E_g. The E_g mode is compatible with a zone-boundary mode, L_3, which plays a role of a soft mode and causes the improper ferroelastic phase transition. The intensity of CM declines in the vicinity of T_C, while it increases at L point. These results reveal the role of each atom. The potassium atom makes a rigid frame, which is evident as the lack of anomaly in the acoustic modes. The rotational motion of tetrahedra contributes largely to the proton conductivity and phase transition. Chaotic rotational motion of SeO_4 tetrahedra with a lifetime of about 10^{-10} s changes into a zone-boundary mode, making local dimer structures with transfer protons in the same time scale.

*Present address: Private, 2-15-11-102 Chikuho, Tsukuba, Ibaraki 300-3253, Japan. fumihito@star.dti2.ne.jp
†kojima@bk.tsukuba.ac.jp

[1] S. M. Haile, D. A. Boysen, C. R. I. Chisholm, and R. B. Merle, Nature (London) **410**, 910 (2001).
[2] Y. Noda, H. Kasatani, Y. Watanabe, and H. Terauchi, J. Phys. Soc. Jpn. **61**, 905 (1992).
[3] C. Totsuji and T. Matsubara, J. Phys. Soc. Jpn. **63**, 2760 (1994).
[4] Y. Suwa, J. Yamaguchi, H. Kageshima, and S. Tsuneyuki, Mater. Sci. Eng., B **79**, 31 (2001).
[5] F. Fillaux, A. Lautié, J. Tomkinson, and G. J. Kearly, Chem. Phys. **154**, 135 (1991).
[6] Y. Moritomo, Y. Tokura, N. Nagaosa, T. Suzuki, and K. Kumagai, Phys. Rev. Lett. **71**, 2833 (1993).
[7] P. Kaung, M. Kasahara, and T. Yagi, J. Phys. Soc. Jpn. **65**, 1114 (1996).
[8] J. Hatori, Y. Matsuo, and S. Ikehata, Solid State Commun. **140**, 452 (2006).
[9] M. Ichikawa, S. Sato, M. Komukae, and T. Osaka, Acta Crystallogr., Sect. C: Cryst. Struct. Commun. **48**, 1569 (1992).
[10] N. Onoda-Yamamuro, O. Yamamuro, T. Matsuo, M. Ichikawa, R. M. Ibbreson, and W. I. F. David, J. Phys.: Condens. Matter **12**, 8559 (2000).
[11] F. Shikanai, K. Tomiyasu, N. Aso, S. Ikeda, and T. Kamiyama, Phys. Rev. B **80**, 144103 (2009).
[12] F. Shikanai, R. Kiyanagi, M. Yonemura, D. Sulistyanintyas, K. Iwase, T. Wuernisha, K. Mori, T. Ishigaki, S. Ikeda, and T. Kamiyama, Physica B **385-386**, 156 (2006).
[13] B. V. Merinov, A. I. Baranov, and L. A. Shuvalov, Sov. Phys. Crystallogr. **35**, 200 (1990).
[14] A. Bohn, R. Melzer, R. Sonntag, R. E. Lechner, G. Schuc, and K. Langer, Solid State Ionics **77**, 111 (1995).
[15] R. E. Lechner, Solid State Ionics **145**, 167 (2001).
[16] N. I. Pavlenko and I. V. Stasyuk, J. Chem. Phys. **114**, 4607 (2001).
[17] H. Kamimura, Y. Matsuo, S. Ikehata, T. Ito, M. Komukae, and T. Osaka, Phys. Status Solidi B **241**, 61 (2004).
[18] S. Yokota, Y. Makita, and Y. Takagi, J. Phys. Soc. Jpn. **51**, 1461 (1982).
[19] F. Shikanai *et al.*, Ferroelectrics **347**, 74 (2007).
[20] F. M. Jiang and S. Kojima, Appl. Phys. Lett. **77**, 1271 (2000).
[21] K. I. Suzuki and S. Hayashi, Phys. Rev. B **73**, 024305 (2006).